



Compact structured silicon/carbon composites as high-performance anodes for lithium ion batteries

Zhewei Yang¹ · Yang Yang¹ · Huajun Guo¹ · Zhixing Wang¹ · Xinhai Li¹ · Yu Zhou¹ · Jiexi Wang¹

Received: 19 December 2017 / Revised: 3 February 2018 / Accepted: 6 February 2018 / Published online: 21 February 2018
© Springer-Verlag GmbH Germany, part of Springer Nature 2018

Abstract

Compact-structured silicon/carbon composites consisting of silicon, graphite, and coal tar pitch pyrolysis carbon are prepared via two heating procedures after liquid solidification. The first heating procedure plays a key role in the formation of compact-structured silicon/carbon composites, in which the coal tar pitch has a good fluidity at 180 °C above the softening temperature, and it is easy to form a uniform coating on the surface of materials. At the same time, the fluidic coal tar pitch could also fill the voids between particles to form compact-structured silicon/carbon composites. As-prepared silicon/carbon composites exhibit moderate reversible capacity of 602.4 mAh g⁻¹, high initial charge-discharge efficiency of 82.3%, and good cycling stability with the capacity retention of 93.4% at 0.1 A g⁻¹ after 50 cycles. It is noteworthy that the synthetic method is scalable which is suitable for mass production.

Keywords Lithium ion batteries · Silicon · Pitch · Composites · Compact structure

Introduction

Nowadays, facing the challenges of ecological environment and natural resources' shortage, it is urgent for all industry to pursue "green" or sustainable development [1–8]. In the field of energy conversion and storage, lithium ion batteries (LIBs) is considered to be one of most efficient energy storage devices which possess high energy density, high power density, and long cycling life [9–13]. The anode material plays an important role in LIB. Graphite, as the dominating anode material for LIBs nowadays, possesses the theory capacity of 372 mAh g⁻¹ which could not satisfy the requirement of LIB with high capacity [14, 15]. Silicon will become a new generation of anode material due to the advantages of high theoretical capacity (4200 mAh g⁻¹) and low lithiation/

delithiation potential [16]. However, silicon has poor cyclic performance because of poor electrical conductivity and large volume expansion (300%) during charge-discharge process [17]. In order to solve these problems, extensive researches have been carried out [18–24]. Designing silicon nanostructures and synthesizing Si-based composite are the primary means. Special silicon nanostructures including nanotube, nanowire, nanosphere, and nanofilm have been reported.

Silicon/carbon composite is one of the most promising composites due to its excellent electrical conductivity and structure stability of carbon [25, 26]. However, most current preparation technologies for Si-based materials are not suited for large-scale production because of the complicated process and the expensive costing. Graphite and coal tar pitch are important carbon sources to synthesize Si/C composite due to high electronic conductivity, excellent cohesiveness, and structure stability. However, simple operation by mixing three raw materials (silicon, graphite, and coal tar pitch) is unable to provide a stable structure because the raw materials could not have a perfect cladding layer.

Herein, compact-structured silicon/carbon composites are prepared via a scalable heating procedure after mixing raw materials. At the temperature (180 °C) over the softening temperature (110 °C), the coal tar pitch has a good fluidity and it is easy to form a uniform coating on the surface of materials. At the same time, the fluidic coal tar pitch could also fill the voids

Zhewei Yang and Yang Yang contributed equally to this work.

Electronic supplementary material The online version of this article (<https://doi.org/10.1007/s11581-018-2486-6>) contains supplementary material, which is available to authorized users.

✉ Huajun Guo
hjguo_csu@163.com

¹ School of Metallurgy and Environment, Central South University, Changsha 410083, People's Republic of China

between particles to form compact-structured silicon/carbon composites, which is in favor of constructing conductive networks. The structure and electrochemical performance are characterized, and the relationship between them is also discussed.

Experimental

Material synthesis

All raw materials were commercial products. Through the theoretical calculation, the specific capacity design of composite should not be more than 867 mAh g^{-1} to avoid over-large electrode volume variation [27]. In this study, the content of the silicon was less than 16%. The precursor was prepared by liquid solidification [28]. The weight ratio of Si, graphite, and coal tar pitch pyrolysis carbon was designed to 15:75:10. Commercial nano-silicon powders (> 99.9%, ~ 80 nm, Zhongning Materials Technology Co., Ltd., Zhejiang, China) was dispersed in ethanol by sonication for 1 h to get a homogeneous dispersed suspension. Then, coal tar pitch (China Power Investment Corporation Ningxia Qingtongxia Energy Aluminum Co., Ltd.) and flake graphite powders (> 99%, ~ 1 μm , Qingdao Tianhe Graphite Co., Ltd., Shandong, China) were dispersed into the above-mentioned suspension by sonication for 2 h. After dispersing uniformly, the mixture was evaporated by stirring at 90°C as the precursor of silicon/carbon composite. At last, the precursor was sintered at two heat-treatment stages in tube furnace and the heating rate is 5°C min^{-1} . The first heat-treatment stage sustained for 4 h at 180°C (S180) in vacuum and the second heat-treatment stage sustained for 3 h at 850°C in Ar. The materials treated at 120°C (S120) and 200°C (S200) during the first heat-treatment stage, and the material without the first heat-treatment stage (S0) were conducted by the same method. The preparation of compact-structured silicon/carbon composites is shown in Scheme 1.

Material characterization

Thermogravimetric (TG) analysis of the precursor was performed on a SDT Q600 TG (TE, USA) apparatus from 0 to

900°C at a heating rate of 5°C min^{-1} in Ar and air atmosphere, respectively. The crystal structure of the composite was characterized by the powder X-ray diffraction (XRD, Rint-2000, Rigaku) in the range of $2\theta = 10^\circ\text{--}80^\circ$. The morphology of the composite was observed by scanning electron microscopy (SEM, JEOL, JSM-5600LV). The microstructure of the composite was examined by a Tecnai G12 transmission electron microscope (TEM). Nitrogen adsorption/desorption isotherms at 77.3 K was obtained using a Micromeritics ASAP 2460 surface area and porosity analyzer. The electronic conductivities of all samples were tested using ST-2722 semiconductor resistivity of the powder tester by four-point probe method.

Electrochemical measurement

The working electrode was made up of active material, Super P, and LA132 binder at a weight ratio of 87:5:8. The slurry dispersed in deionized water was spread on a copper foil and dried at 80°C for 4 h in a vacuum-drying chamber. Electrodes were punched in the form of 12-mm-diameter disks. The thickness of electrode was controlled by the coating machine, and the mass of the active materials was kept around 1.2 mg. The button cells were carried out in an argon-filled glove box using 1 M LiPF_6 in a mixture of EC/EMC/DMC (1:1:1 by volume) as the electrolyte. The electrochemical performances of button cells were tested by a Neware Battery Test System with a cut-off voltage range from 0.01 to 2.00 V (vs. Li/Li^+) at room temperature. Cyclic voltammetry (CV) was recorded using a CHI660A electrochemical analyzer at a scanning rate of 0.1 mV s^{-1} . Electrochemical impedance spectroscopy (EIS) was performed using a CHI660A electrochemical analyzer by applying 5 mV AC voltage in the frequency range of $10^{-2}\text{--}10^5 \text{ Hz}$.

Results and discussion

Material characterizations

Thermogravimetric (TG) analysis of the precursors was performed in Ar, and the result is shown in Fig. 1a. The weight loss of precursor corresponds to the pyrolysis of the coal tar

Scheme 1 Preparation of compact structured silicon/carbon composites

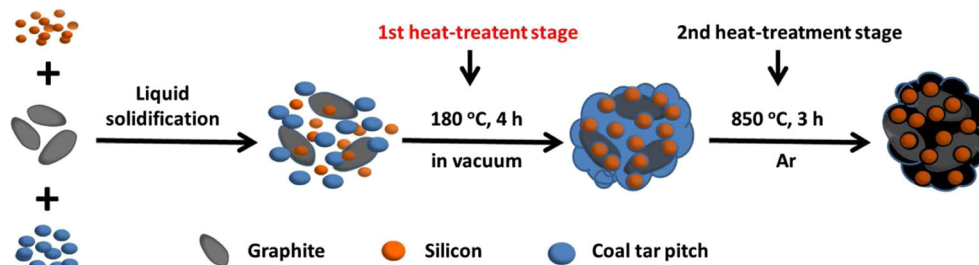
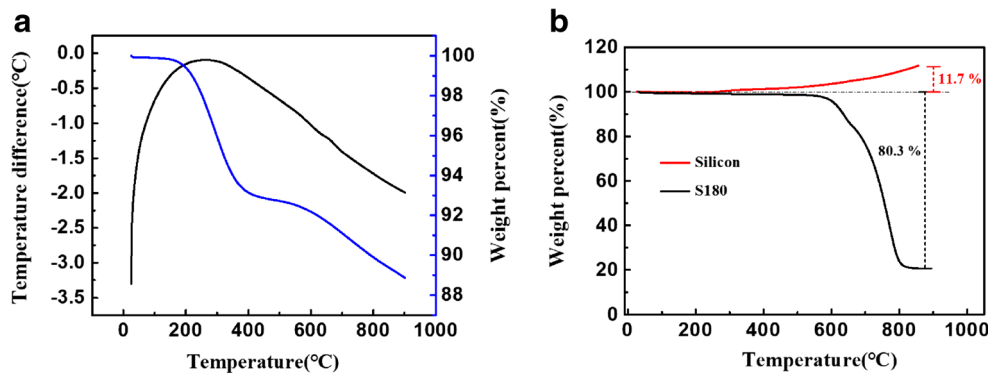


Fig. 1 **a** TG curve of the precursor in Ar. **b** TG curves of the composite S180 and silicon in air



pitch, because graphite and Si are steady in argon atmosphere below 900 °C [29]. There is a little weight loss between 0 and 200 °C, which is resulted from the removal of the absorbed water in the coal tar pitch. The large weight loss from 200 to 900 °C is due to the decomposition of coal tar pitch including the release of low-molecular-weight hydrocarbons, polycondensation of aromatic molecules, and so on. The mass loss rate is changeless above 550 °C. The pyrolysis temperature is designed at 850 °C to obtain silicon/carbon composites, and the yield of the precursor retains 89.4%. TG analysis was also carried out in air atmosphere to determine the content of silicon in composite S180. Figure 1b shows the TG curves of S180 and bare silicon in air atmosphere. The weight ratio of bare silicon sample increases to 111.7 wt% at 850 °C due to the oxidation of silicon under air atmosphere, while that of S180 to 19.7 wt% due to the oxidation reaction of carbon to produce carbon oxide gas. Based on these mass loss percentage data, the silicon content is calculated to be approximately 16.7% which is slightly higher than the designed result. And the carbon content is approximately 83.3%.

The XRD patterns of silicon/carbon composites are shown in Fig. 2. It is clear that four samples have the same features corresponding to silicon and graphite. The peaks at around 26.4°, 42.5°, 44.5°, 54.5°, and 78.5° are related to the (002), (100), (101), (004), and (110) diffractions of graphite (PDF no. 08-0415). The peaks at 28.4°, 47.3°, and 56.1° are correlated with the (111), (220), and (311) diffractions of silicon (PDF no. 27-1402) [30]. There is no other phase in the XRD patterns which indicates that the silicon/carbon composites are the blend of silicon, graphite, and amorphous coal tar pitch pyrolysis carbon.

The surface morphologies of silicon/carbon composites are illustrated by SEM (as shown in Fig. S1). The result shows that morphologies of the whole silicon/carbon composites are irregular and micron-sized particles. There are much more silicon particles distributing in the composite S180 (Fig. S1C) than other composites illustrating well integration between silicon, graphite, and coal tar pitch pyrolysis carbon. Figure 3 presents the morphology, element distribution, and microstructure of the silicon/carbon composite S180. As

shown in Fig. 3a–c, S180 shows the irregular morphology, and the silicon and carbon elements are distributed uniformly on the particle surface, which demonstrates that all the raw materials are dispersed well in the composite. TEM and HRTEM are combined to further discern the microstructure of S180. It could be seen that nano-silicon particles with the size of ~80 nm are compactly embedded in the matrix (Fig. 3d). As shown in Fig. 3e, the crystalline plane spacing of 0.336 and 0.313 nm corresponding to graphite (002) and silicon (111), respectively, is observed in HRTEM image (Fig. 3e). Additionally, the amorphous structure marked in yellow cycles is observed not only in the carbon layer but also in the interspace between graphite and silicon which is ascribed to the filling the voids between particles by fluidic coal tar pitch over the softening temperature.

In order to further determine the compactness and connection between all components in all samples, the specific surface area (SSA) was obtained by the Brunauer-Emmett-Teller equation according to nitrogen adsorption/desorption isotherms as shown in Fig. 4. Meanwhile, the textural properties of all samples are shown in Table 1. In Fig. 4, type II isotherms

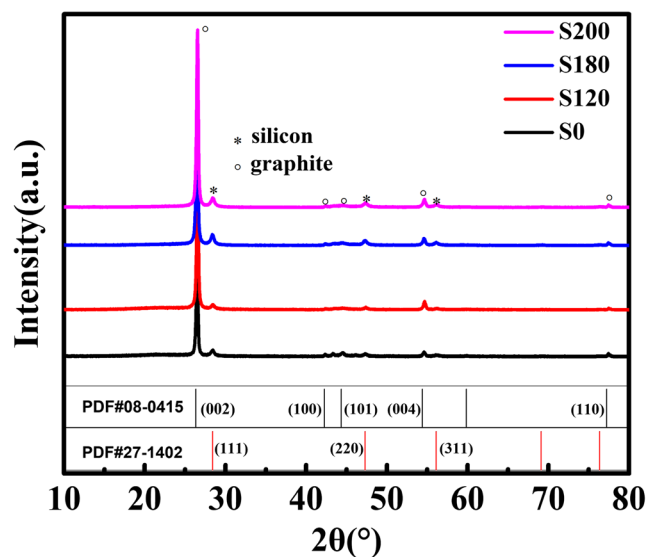


Fig. 2 X-ray diffraction patterns of the samples with different treatments

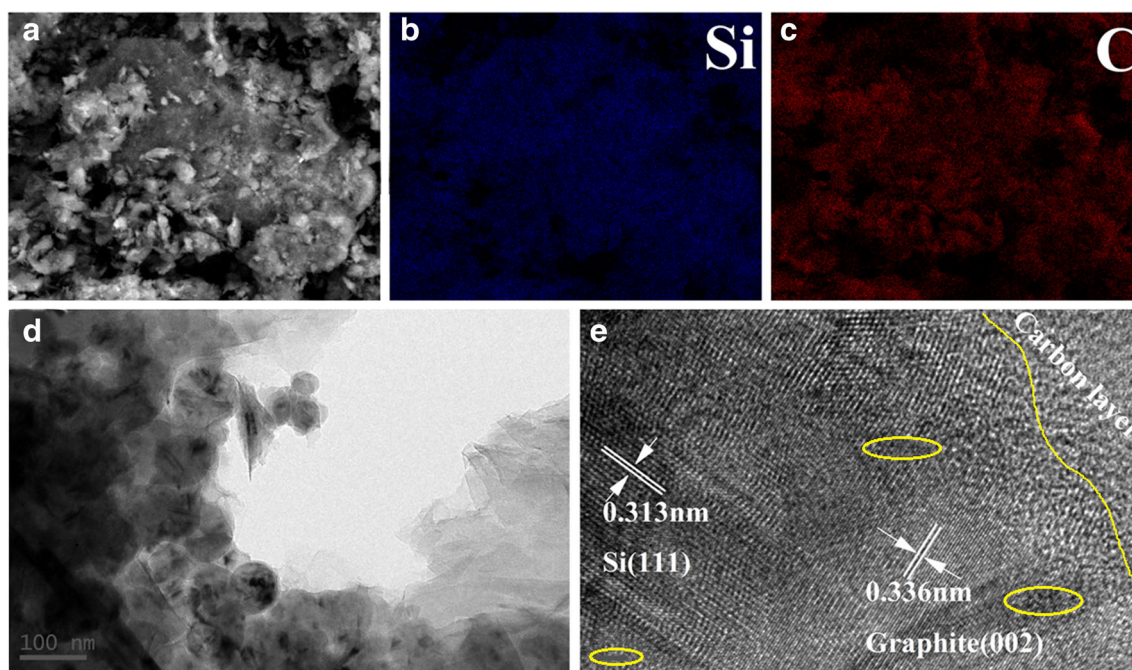


Fig. 3 **a** SEM image. **b**, **c** EDAX spectra dots. **d** TEM image. **e** HRTEM image of sample S180

could be observed for S0, S120, S180, and S200, which indicates that four samples mainly contain large pores and have small SSA. The SSA and pore volume are decreased with the increase of temperature at the first heat-treatment stage. S180 has a smaller SSA of $4.0 \text{ m}^2 \text{ g}^{-1}$ and a pore volume of $0.056 \text{ cm}^3 \text{ g}^{-1}$ than S0 with an SSA of $7.9 \text{ m}^2 \text{ g}^{-1}$ and a pore volume of $0.059 \text{ cm}^3 \text{ g}^{-1}$. It demonstrates that the fluidic coal tar pitch at the first heat-treatment period fills the voids between particles reducing the SSA area and the pore volume.

Electrochemical performance

Electrochemical measurements were carried out at room temperature. Figure 5a displays the first charge-discharge curves

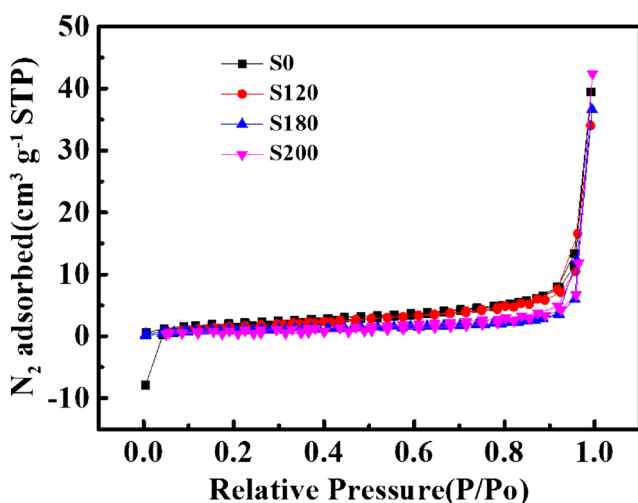


Fig. 4 Nitrogen adsorption/desorption isotherm linear plot of all samples

of all the composites at 0.1 A g^{-1} . The initial reversible capacities of S0, S120, S180, and S200 are 805.7, 705.6, 602.4, and 591.8 mAh g^{-1} , respectively. And the corresponding initial charge-discharge efficiencies are 82.0, 83.1, 82.3, and 84.7%, respectively. Compared with S0, S180 displays lower capacity and slightly higher initial charge-discharge efficiency due to lower SSA and more compact structure probably.

Figure 5b presents the cyclic stability of all samples at 0.1 A g^{-1} for 50 cycles. S180 displays excellent cycle performance, of which the capacity retention could reach 93.4% (562 mAh g^{-1}) after 50 cycles. S200, S120, and S0 could reach 91.1, 57.6, and 36.8%, respectively. Even at high current density of 1 A g^{-1} as shown in Fig. S2, the capacity retention of S180 could keep 71.5% (343 mAh g^{-1}) after 100 cycles, which is higher than others. The rate capabilities of S0, S120, S180, and S200 at 0.1, 0.2, 0.5, 1, and 2 A g^{-1} are presented in Fig. 5c. At 0.1 A g^{-1} , the charge capacities (3rd cycle) of S0, S120, S180, and S200 are 730, 652, 607, and 596 mAh g^{-1} ,

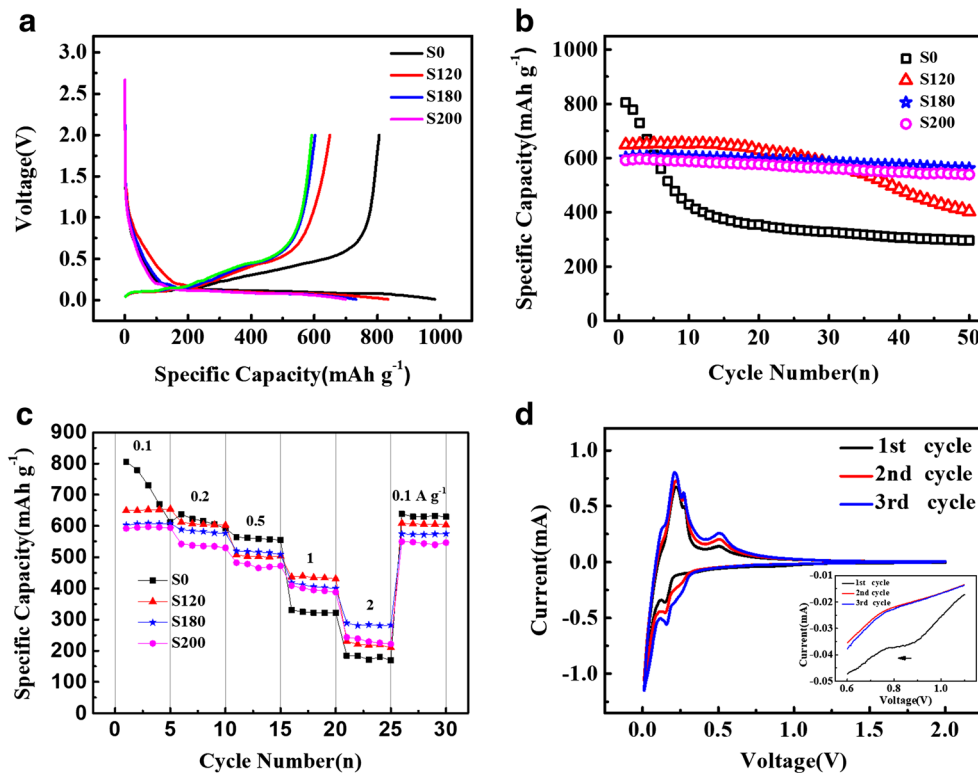
Table 1 Textural properties and electronic conductivities of all samples

Samples	$S_{\text{BET}}^{\text{a}}$ ($\text{m}^2 \text{ g}^{-1}$)	V_{t}^{b} ($\text{cm}^3 \text{ g}^{-1}$)	Conductivity (S m^{-1})
S0	7.9	0.059	2638
S120	7.7	0.057	2874
S180	4.0	0.056	3246
S200	2.2	0.043	3322

^a The specific surface area (SSA) was calculated by BET equation

^b The total pore volume (TPV) was obtained at relative pressure $p/p_0 = 0.99$

Fig. 5 **a** The first charge-discharge curves of all samples at 0.1 A g^{-1} . **b** Cycling profiles of all samples at 0.1 A g^{-1} . **c** Rate capability of all samples. **d** CV curves of the sample S180 for the first 3 cycles at the scanning rate of 0.1 mV s^{-1} . Inset: CV curves at high magnification



respectively. With the rise of current density, the capacity decreases. At 2 A g^{-1} , S180 exhibits the capacity retention of 46% with respect to initial capacity at 0.1 A g^{-1} , which is higher than that of S0 (23%), S120 (33%), and S200 (38%). S180 possesses favorable cyclic stability and rate capability due to the compact structure. The graphite served as good

dispersive matrix for silicon contributes to high electronic conductivity for the silicon/carbon composite. The amorphous structure derived from coal tar pitch in the carbon layer and the interspace between graphite and silicon not only buffers the volume change of silicon but also connects graphite with silicon to construct conductive networks. Compared with the

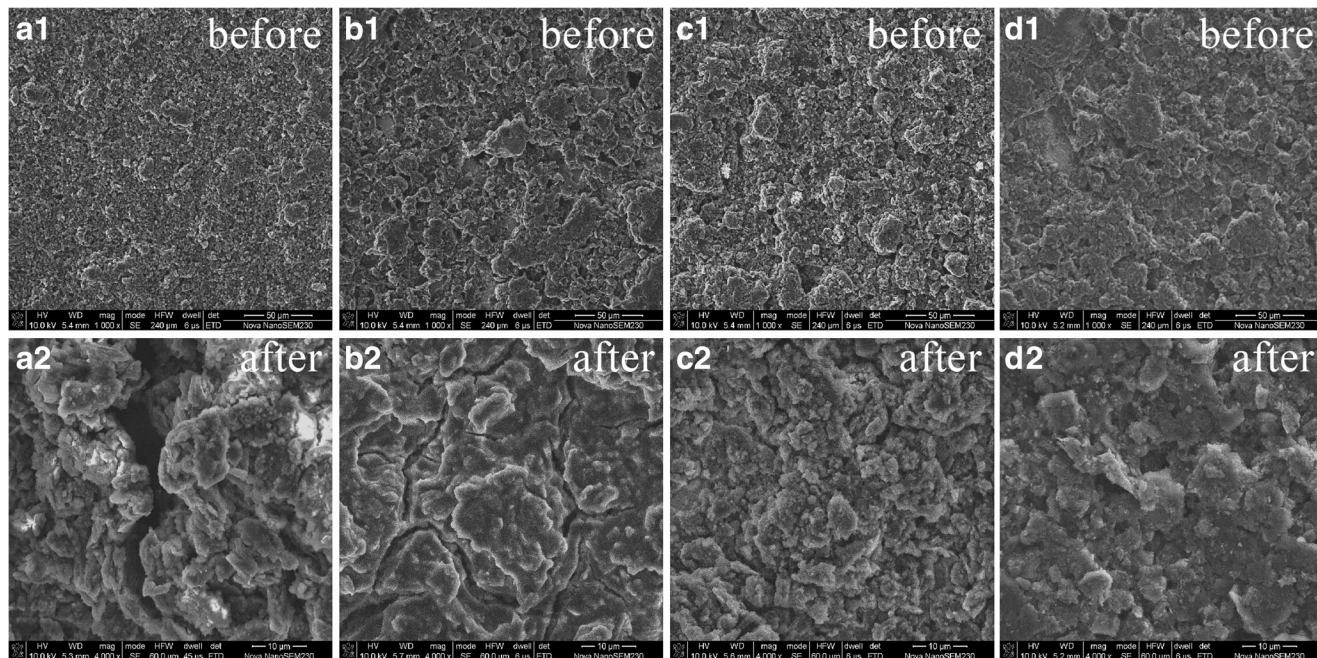


Fig. 6 SEM images of electrodes before and after 50 cycles for sample S0 (a1) and (a2); sample S120 (b1) and (b2); sample S180 (c1) and (c2); sample S200 (d1) and (d2)

silicon/carbon composites consisting of silicon, graphite, and pitch pyrolysis carbon reported in literature (Table S1) [31–34], our silicon/carbon composites have competitive electrochemical performances. Additionally, the preparation method is simple and practicable, which is suitable for mass production.

Figure 5d shows the CV curves of S180 for the first 3 cycles at 0.1 mV s^{-1} . As shown in inset, the broad cathodic peak at around $\sim 0.8 \text{ V}$ appears in the first cycle but disappears in the following two cycles, which is related to the formation of SEI layer on the surface of electrode due to the decomposition of electrolyte [35]. The reduction peaks between 0.01 and 0.25 V correspond to the lithium intercalation into graphite and alloying action with silicon. The oxidation peaks at 0.15 and 0.18 V correspond to the deintercalation of lithium ions into graphite while peaks at 0.25 and 0.49 V correspond to the dealloying process of silicon [36].

Additionally, we also characterize the morphologies of electrodes before and after cycling for 50 cycles at 0.1 A g^{-1} . As shown in Fig. 6, there are obvious cracks on the electrodes of S120 and S0 after cycling, while the electrodes of samples S180 and S200 are still integrated. It is proved that the first heating procedure plays a key role in the formation of compact structured silicon/carbon composites, which is conducive to the cyclic stability of materials.

The EIS measurements are conducted after initial cycling. The Nyquist plots of all samples are shown in Fig. 7, which consist of a semicircle at high frequency and a linear slope at low frequency corresponding to the charge transfer resistance (R_2) and the Warburg resistance (W_0), respectively [37]. In addition, the intercept along X-axis indicates the electrolyte resistance (R_1). The plots are fitted with the aid of an appropriate electric equivalent circuit as shown in the inset of Fig. 7, and the fitting dates are shown in Table 2. It could obviously be seen that S200 and S180 possessed smaller R_1 and R_2 than S120 and S0, which indicates higher exchange current density

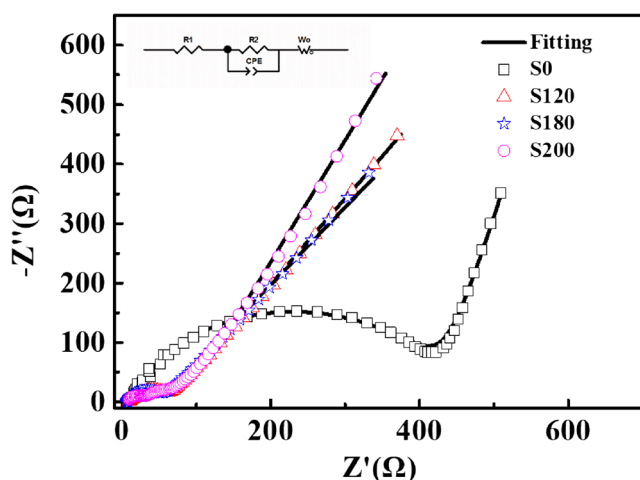


Fig. 7 Nyquist plots of all samples after the initial cycle

Table 2 Electrochemical impedance parameters of samples

Sample	$R_1(\Omega)$	$R_2(\Omega)$
S0	10.77	418.60
S120	9.51	53.89
S180	6.57	42.14
S200	4.75	22.88

and higher electronic conductivity. The same results could also be confirmed by actual electronic conductivities of all samples. As shown in Table 1, the electronic conductivities of S0, S120, S180, and S200 are 2638, 2874, 3246, and 3322 S m^{-1} . S200 and S180 possess higher electronic conductivity than S120 and S0, which is ascribed to that the coal tar pitch with a good fluidity at the temperature over the softening temperature is able to connect graphite with silicon to construct conductive networks.

Conclusions

In summary, the compact-structured silicon/carbon composites with high electrochemical performance were synthesized by sintering at two heat-treatment procedures (at $180 \text{ }^\circ\text{C}$ for 4 h and at $850 \text{ }^\circ\text{C}$ for 3 h). The specific surface area and pore volume were reduced due to the filling the voids between particles by fluidic coal tar pitch at the first heat-treatment stage. As-prepared silicon/carbon composites exhibited good electrochemical performance due to the compact structure. The results indicate that the preparation method sintering at two heat-treatment periods could be a promising method for silicon/carbon composites.

Funding information This work was financially supported by the National Science and Technology Support Program of China (2015BAB06B00), the Program of Strategic Emerging Industries of Hunan Province, China (Grant No. 2017GK4019), and the Fundamental Research Funds for the Central Universities of Central South University (No. 2017zzts126). Additionally, we thank the financial supporting from the collaborative Innovation Center of Manganese-Zinc-Vanadium Industrial Technology (the 2011 plan of Hunan province).

References

1. Goodenough JB, Park KS (2013) The Li-ion rechargeable battery: a perspective. *J Am Chem Soc* 135(4):1167–1176
2. Wang T, Zhang L, Li C, Yang W, Song T, Tang C, Meng Y, Dai S, Wang H, Chai L (2015) Synthesis of core-shell magnetic Fe_3O_4 @poly(m-phenylenediamine) particles for chromium reduction and adsorption. *Environ Sci Technol* 49(9):5654–5662
3. Yang Z, Guo H, Li X, Wang Z, Yan Z, Wang Y (2016) Natural sisal fibers derived hierarchical porous activated carbon as capacitive material in lithium ion capacitor. *J Power Sources* 329:339–346
4. Chai LY, Wang QW, Li QZ, Yang ZH, Wang YY (2010) Enhanced removal of Hg(II) from acidic aqueous solution using thiol-functionalized biomass. *Water Sci Technol* 62(9):2157–2166

5. Li T, Li X, Wang Z, Guo H (2017) A short process for the efficient utilization of transition-metal chlorides in lithium-ion batteries: a case of $\text{Ni}_{0.8}\text{Co}_{0.1}\text{Mn}_{0.1}\text{O}_{1.1}$ and $\text{LiNi}_{0.8}\text{Co}_{0.1}\text{Mn}_{0.1}\text{O}_2$. *J Power Sources* 342:495–503
6. Xu F, Xu J, Xu H, Lu Y, Yang H, Tang Z, Lu Z, Fu R, Wu D (2017) Fabrication of novel powdery carbon aerogels with high surface areas for superior energy storage. *Energy Storage Mater* 7:8–16
7. Wang J, Zhang G, Liu Z, Li H, Liu Y, Wang Z, Li X, Shih K, Mai L (2018) $\text{Li}_3\text{V}(\text{MoO}_4)_3$ as a novel electrode material with good lithium storage properties and improved initial coulombic efficiency. *Nano Energy* 44:272–278
8. Tan L, Li X, Wang Z, Guo H, Wang J (2018) Lightweight reduced graphene oxide@ MoS_2 interlayer as polysulfide barrier for high-performance lithium-sulfur batteries. *ACS Appl Mater Interfaces* 10(4):3707–3713
9. Yan Z, Hu Q, Yan G, Li H, Shih K, Yang Z, Li X, Wang Z, Wang J (2017) $\text{Co}_3\text{O}_4/\text{Co}$ nanoparticles enclosed graphitic carbon as anode material for high performance Li-ion batteries. *Chem Eng J* 321: 495–501
10. Ji L, Lin Z, Alcoutlabi M, Zhang X (2011) Recent developments in nanostructured anode materials for rechargeable lithium-ion batteries. *Energy Environ Sci* 4(8):2682–2699
11. Yan G, Li X, Wang Z, Guo H, Xiong X (2014) Beneficial effects of 1-propylphosphonic acid cyclic anhydride as an electrolyte additive on the electrochemical properties of $\text{LiNi}_{0.5}\text{Mn}_{1.5}\text{O}_4$ cathode material. *J Power Sources* 263(5):231–238
12. Chen S, Shen L, van Aken PA, Maier J, Yu Y (2017) Dual-functionalized double carbon shells coated silicon nanoparticles for high performance lithium-ion batteries. *Adv Mater* 29(21): 1605650
13. Zheng J, Han Y, Sun D, Zhang B, Cairns EJ (2017) In situ-formed $\text{LiVPO}_4@ \text{V}_2\text{O}_5$ core-shell nanospheres as a cathode material for lithium-ion cells. *Energy Storage Mater* 7:48–55
14. Yang Z, Guo H, Li X, Wang Z, Wang J, Wang Y, Yan Z, Zhang D (2017) Graphitic carbon balanced between high plateau capacity and high rate capability for lithium ion capacitors. *J Mater Chem A* 5(29):15302–15309
15. Hou H, Banks CE, Jing M, Zhang Y, Ji X (2015) Carbon quantum dots and their derivative 3D porous carbon frameworks for sodium-ion batteries with ultralong cycle life. *Adv Mater* 27(47):7861–7866
16. Liu N, Lu Z, Zhao J, McDowell MT, Lee HW, Zhao W, Cui Y (2014) A pomegranate-inspired nanoscale design for large-volume-change lithium battery anodes. *Nat Nanotechnol* 9(3): 187–192
17. Hui W, Yi C (2012) Designing nanostructured Si anodes for high energy lithium ion batteries. *Nano Today* 7(5):414–429
18. Chan CK, Peng H, Liu G, Mcilwrath K, Zhang XF, Huggins RA, Cui Y (2008) High-performance lithium battery anodes using silicon nanowires. *Nat Nanotechnol* 3(1):187–191
19. Davenas J, Dkhil SB, Cornu D, Rybak A (2012) Silicon nanowire/P3HT hybrid solar cells: effect of the electron localization at wire nanodiameters. *Energy Procedia* 31(31):136–143
20. Wen Z, Lu G, Mao S, Kim H, Cui S, Yu K, Huang X, Hurley PT, Mao O, Chen J (2013) Silicon nanotube anode for lithium-ion batteries. *Electrochem Commun* 29(10):67–70
21. Menon M, Andriotis AN, Froudakis G (2014) Structure and stability of Ni-encapsulated Si nanotube. *Nano Lett* 2(4):301–304
22. Hong SC, Lee JG, Lee HY, Sang WK, Chong RP (2011) Effects of surrounding confinements of Si nanoparticles on Si-based anode performance for lithium ion batteries. *Electrochim Acta* 56(2): 790–796
23. Zhang YQ, Xia XH, Wang XL, Mai YJ, Shi SJ, Tang YY, Gu CG, Tu JP (2012) Three-dimensional porous nano-Ni supported silicon composite film for high-performance lithium-ion batteries. *J Power Sources* 213(9):106–111
24. Zhou Y, Guo H, Yong Y, Wang Z, Li X, Zhou R (2017) Introducing reduced graphene oxide to improve the electrochemical performance of silicon-based materials encapsulated by carbonized polydopamine layer for lithium ion batteries. *Mater Lett* 195:164–167
25. Zhou Y, Guo H, Yang Y, Wang Z, Li X, Zhou R, Peng W (2016) Facile synthesis of silicon/carbon nanospheres composite anode materials for lithium-ion batteries. *Mater Lett* 168(20):138–142
26. Yong NJ, Kim Y, Kim JS, Song JH, Kim KJ, Chong YK, Dong JL, Park CW, Kim YJ (2010) Si-graphite composites as anode materials for lithium secondary batteries. *J Power Sources* 195(18): 6031–6036
27. Luo F, Liu B, Zheng J, Geng C, Zhong K, Li H, Huang X, Chen L (2015) Review—nano-silicon/carbon composite anode materials towards practical application for next generation Li-ion batteries. *J Electrochem Soc* 162(14):A2509–A2528
28. Su M, Wang Z, Guo H, Li X, Huang S, Gan L (2013) Silicon, flake graphite and phenolic resin-pyrolyzed carbon based Si/C composites as anode material for lithium-ion batteries. *Adv Powder Technol* 24(6):921–925
29. Ng SH, Wang J, Konstantinov K, Wexler D, Chew SY, Guo ZP, Liu HK (2007) Spray-pyrolyzed silicon/disordered carbon nanocomposites for lithium-ion battery anodes. *J Power Sources* 174(2): 823–827
30. Yang Y, Wang Z, Yan G, Guo H, Wang J, Li X, Zhou Y, Zhou R (2017) Pitch carbon and LiF co-modified Si-based anode material for lithium ion batteries. *Ceram Int* 43(12):8590–8595
31. Zhou R, Fan R, Tian Z, Zhou Y, Guo H, Kou L, Zhang D (2016) Preparation and characterization of core-shell structure Si/C composite with multiple carbon phases as anode materials for lithium ion batteries. *J Alloy Compd* 658:91–97
32. Li M, Hou X, Sha Y, Wang J, Hu S, Liu X, Shao Z (2014) Facile spray-drying/pyrolysis synthesis of core-shell structure graphite/silicon-porous carbon composite as a superior anode for Li-ion batteries. *J Power Sources* 248:721–728
33. Li J, Wang J, Yang J, Ma X, Lu S (2016) Scalable synthesis of a novel structured graphite/silicon/pyrolyzed-carbon composite as anode material for high-performance lithium-ion batteries. *J Alloy Compd* 688:1072–1079
34. Yang Y, Wang Z, Zhou Y, Guo H, Li X (2017) Synthesis of porous Si/graphite/carbon nanotubes@ C composites as a practical high-capacity anode for lithium-ion batteries. *Mater Lett* 199:84–87
35. Shim J, Striebel KA (2004) The dependence of natural graphite anode performance on electrode density. *J Power Sources* 130(1): 247–253
36. Shi L, Wang W, Wang A, Yuan K, Jin Z, Yang Y (2016) Scalable synthesis of core-shell structured SiO_x /nitrogen-doped carbon composite as a high-performance anode material for lithium-ion batteries. *J Power Sources* 318:184–191
37. Zhou R, Guo H, Yang Y, Wang Z, Li X, Zhou Y (2016) N-doped carbon layer derived from polydopamine to improve the electrochemical performance of spray-dried Si/graphite composite anode material for lithium ion batteries. *J Alloys Compd* 689:130–137